scientific reports

Check for updates

OPEN

Novel dual action chimera doxorubizen demonstrates superior efficacy to doxorubicin in acute leukemia

Dipak Walunj[1,7], Katarina Egarmina[2,3,7], Adi Zipin-Roitman[4], Siva Sai Naga Anurag Muddineni[1], Iryna Tkachenko[1], Pousali Mitra[1], Dror Tobi[2], Andrii Bazylevich[1], Ofer Shpilberg[5,6], Michael Milyavsky[4,7]✉, Oshrat Hershkovitz-Rokah[2,3,7]✉ & Gary Gellerman[1,7]✉

Modifying existing drugs to enhance their activity and reduce toxicity is a major focus of drug development. We developed a novel class of dual-action chimeric molecules for cancer therapy, linking known drugs to a DNA-methylating monomethyl triazene moiety (azene) via nucleophilic substitution. In-vitro screening of these chimeras on various leukemia cell lines identified a potent chimera, doxorubizen, a sequel of the known DNA intercalator and topoisomerase 2 (Topo-II) inhibitor doxorubicin (Dox) and azene. Molecular docking and dynamic simulations showed doxorubizen as a more potent Topo-II inhibitor than Dox as it binds to major grooves in DNA. Moreover, the monomethyl triazene portion is positioned favorably through tetracene core intercalation, potentially facilitating methylation at nearby guanine bases. Doxorubizen demonstrated significantly higher cytotoxicity, mitochondrial depolarization, DNA intercalation, and cell death than Dox. A Topo-II activity assay confirmed potent enzyme inhibition by doxorubizen. The mechanism of action of doxorubizen involves the inhibition of DNA repair in proximity to double-strand breaks by guanine methylation, enhanced mitochondrial depolarization, and increased apoptosis. Furthermore, in an acute leukemia xenograft model, doxorubizen significantly reduced the leukemia burden compared to Dox while preserving body weight and liver function. This work underscores the therapeutic potential of doxorubizen in leukemia treatment.

Keywords Anticancer drug, DNA intercalation, DNA double-strand breaks, Molecular

A popular approach to drug design involves modifying currently approved drugs to boost their anticancer efficacy and minimize side effects. One common way to address this task is by creating structural hybrids (chimeras) of drugs, merging their pharmacophores into one dual-action molecular entity[1]. These molecular chimeras simultaneously target several locations in cellular systems, and numerous substances for anticancer applications have been extensively explored in recent years[2–4]. More examples can be found in Ohsawa et al. and Yan et al.'s works. Ohsawa et al. synthesized estrabucil by conjugating estradiol with chlorambucil (CLB)[5], creating a structural hybrid in which estradiol acts as the vehicle, directing the chimera to estrogen receptor-positive tumors. Yan et al. performed direct conjugation between hydrophilic irinotecan and hydrophobic CLB to obtain an amphiphilic conjugate that self-assembled into nanoparticles[6]. However, cancer resistance can arise through numerous cell defense mechanisms, such as excessive drug efflux or reduced drug uptake, target al.terations, drug inactivation, DNA damage repair, and apoptotic pathway blockade[7–11]. Thus, it would be very advantageous to develop new chimeric compounds with increased anticancer activity. To elaborate on the evolution of new chimeric drug entities, we decided to conjugate known anticancer drugs with the DNA-methylating monomethyl triazene moiety protected by methyl carbamate (**azene**) *via*a self-immolative

[1]Department of Chemical Sciences, Ariel University, PO Box 3, Ariel 40700, Israel. [2]Department of Molecular Biology, Ariel University, Ariel, Israel. [3]Translational Research Lab, Assuta Medical Center, Tel Aviv, Israel. [4]Department of Pathology, Faculty of Medical & Health Sciences, Tel-Aviv University, Tel- Aviv, Israel. [5]Adelson School of Medicine, Ariel University, Ariel, Israel. [6]Institute of Hematology, Assuta Medical Center, Tel Aviv, Israel. [7]Dipak Walunj, Katarina Egarmina, Michael Milyavsky, Oshrat Hershkovitz-Rokah and Gary Gellerman contributed equally. ✉email: mmilyavsky@post.tau.ac.il; oshratr@assuta.co.il; garyg@ariel.ac.il

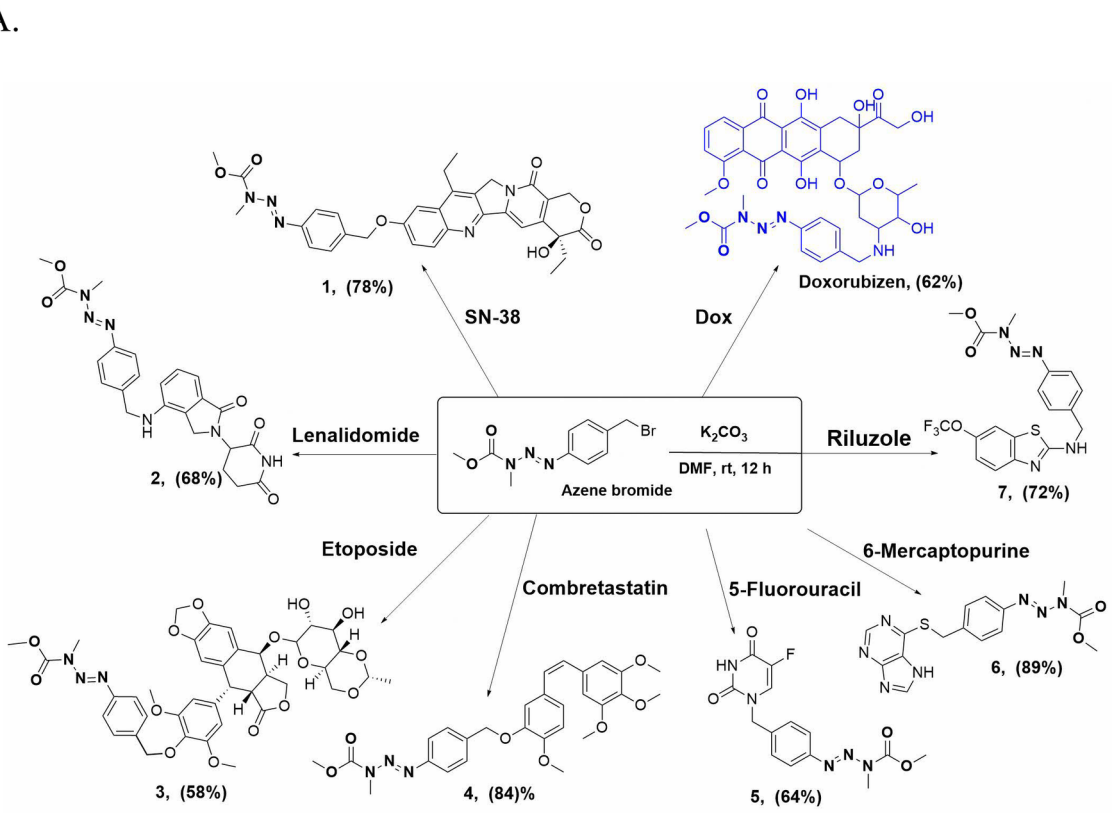

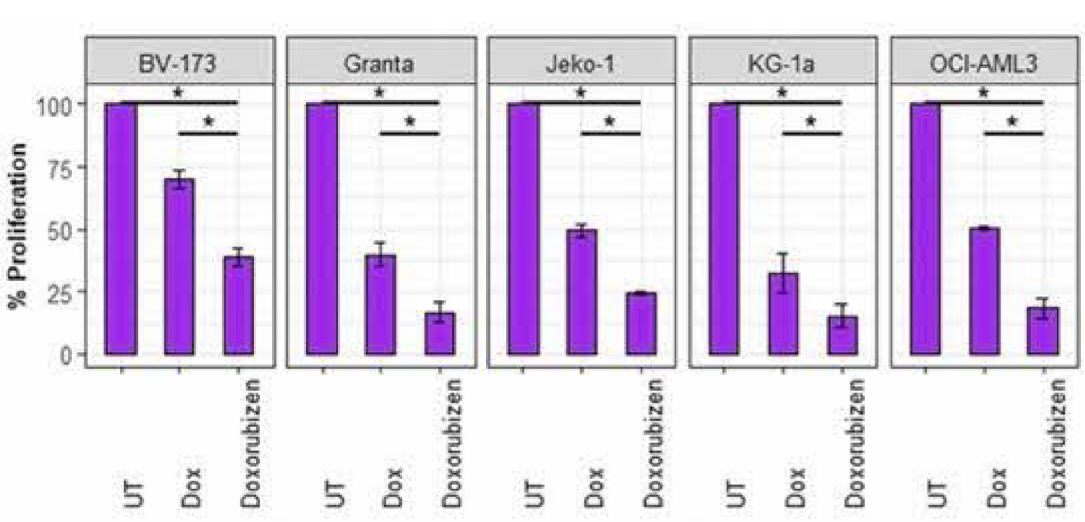

Fig. 1. **Synthesis and biological activity of doxorubizen. (A)** Synthesis of **doxorubizen** and chimeras **1**–**7**. **(B) The cytotoxic effects of doxorubizen were compared to those of the parental drug Dox**. BV-173, Granta, Jeko-1, KG-1a, and OCI-AML3 cells were treated with doxorubicin (dox) or **doxorubizen** for 48 h at 50 nM each. The proliferation rate was measured by the WST-1 assay. The graphs represent the means ± SEMs from at least 3 experiments; $^{*}p < 0.05$. SEM: standard error of the mean; UT: untreated.

p-aminobenzyl (PAB) linker[4] (Fig. 1A). We assumed that upon cleavage of the carbamate protecting group of the chimera in proximity to the active site, the methyl carbocation (Me^{+}) will be released, liberating the parent drug from the self-immolative linker, and both the drug and Me^{+}will interact with the corresponding intracellular biophore target[12]. We previously used **azene**to anchor the amonafide backbone of amonafidazene, a chimera that greatly amplifies the generation of DNA double strand breaks (DSBs) and significantly slows DSB repair compared to the effects of amonafide alone in the submicromolar range, indicating that methylation in proximity to DSBs indeed suppresses DNA repair processes[4,13]. Based on the above, we decided to link the **azene**bromide tether[14]to a series of known mechanistically different anticancer drugs and evaluate the resulting 'chimeric' biological

effectiveness vs. parent drugs. We focused on the following: (1) the DNA intercalator and Topo II inhibitor doxorubicin (Dox); (2) the Topo II inhibitor etoposide; (3) the microtubule inhibitor combretastin; (4) the Topo I inhibitor SN-38; (5) the antimetabolites 5-fluorouracil and 6-mercaptopurine; (6) the antiangiogenic agent lenalidomide; and (7) a neuroprotective drug with potential as a novel anticancer agent, riluzole[15] (Fig. 1A). Notably, lenalidomide[16,17], etoposide[18–20], 6-mercaptopurine[21], and doxorubicin[22–25] are used as part of the treatment protocol for hematological malignancies. Therefore, the obtained small library of chimeric substances was screened on various hematological cell lines. One chimera, **doxorubizen**, a hybrid of Dox and **azene**, was found to be the most potent against all the tested cell lines in the nanomolar range, significantly enhancing cytotoxicity, apoptosis, and mitochondrial depolarization over an equimolar concentration of the parent drug Dox. Furthermore, compared with the parental drug, **doxorubizen** demonstrated notable antileukemia effectiveness in vivo. We assumed that, like the previously reported chimera amonafidazene, **doxorubizen**inhibits DNA repair in proximity to double strand breaks (DSBs) by guanine methylation, enhancing cancer cell growth suppression. While Dox is an effective drug, it is associated with several limitations and potential side effects, including cardiotoxicity, bone marrow suppression, and an increased risk of secondary cancers[26,27]. The results presented in this work justify further preclinical evaluation of the effects of **doxorubizen**on broad-scope hematopoietic malignancies, including the degree of dilated cardiomyopathy[28].

Materials and methods

Instruments and general information

Drugs and other reagents were purchased from Tzamal D-Chem Laboratories Ltd., Petah-Tikva, Israel. Chemical reactions were monitored by TLC (Silica gel 60 F-254, Merck)[1]. H and ^{13}C NMR spectra were measured by using a 400 MHz Bruker Avance III HD(^{1}H 400 MHz and ^{13}C 100 MHz) spectrometer in CD_3OD and DMSOd6. All the solvents used were obtained from Bio-Lab Ltd., Jerusalem, Israel, or Gas Technologies Ltd., Kefar Saba, Israel. All other chemicals were obtained from Holland Moran or Sigma–Aldrich. HRMS was performed in ESI-positive mode by using an Agilent 6550 iFunnel Q-TOF LC–MS instrument. IR spectra were recorded as KBr tablets on a Bruker FTIR ALPHA II spectrometer equipped with a platinum diamond attenuated total reflectance (ATR) module. The compounds were purified via normal-phase silica gel chromatography (Silica Flash P60) supplied by Merck. The column was kept at room temperature. The eluents were petroleum ether, ethyl acetate, chloroform, and methanol. Electron spray mass spectra (ESI-MS) were obtained using an Autoflex III smart-beam (MALDI, Bruker), a Q-TOF micro (Waters), or an LCQ Fleet™ ion trap mass spectrometer (Finnigan/Thermo). HPLC/LC–MS analyses were performed using an Agilent infinity 1260 connected to an Agilent quadruple LC–MS 6120 series instrument equipped with a ZORBAX SB-C18 column (2.1 × 50 mm, 1.8 mm). In all the cases, the eluent was composed of A (0.1% FA in H_2O) or B (0.1% FA in ACN), and the elution gradient profile was 100% A for the first 3 min, followed by 5 min (from 3 to 8 min), during which 100% B was reached; this was followed by 5 min (from 8 to 13 min) of 100% B, followed by 2 min (from 13 to 15 min), during which the mixture was returned to A, followed by 2 min (from 15 to 17 min) of 100% A. The UV detection was at 254 nm. The column temperature was maintained at 50 °C. The flow rate was 0.3 mL/min.

General procedure for the synthesis of chimeras

The starting drug (doxorubicin, SN-38, lenalidomide, etoposide, combretastatin, 5-fluorouracil, 6-mercaptopurine, riluzole; 50 mg, 1 equiv. each) was dissolved in dry DMF (5 mL) under a nitrogen atmosphere, and the reaction mixture was cooled to 0 °C. K_2CO_3 (3 equiv.) was added, and the reaction mixture was stirred at 0 °C for 15 min. Then, **azene**bromide[14] (1.2 equiv.) was added dropwise to the mixture, and the mixture was stirred at room temperature for 12 h. After completion of the reaction (monitoring by TLC), the reaction mixture was quenched with water (10 mL) and extracted with CH_2Cl_2 (2 × 20 mL). The organic phase was dried over Na_2SO_4 and then filtered. The solvent was removed using a rotary evaporator, and the crude material was purified by silica gel chromatography.

(E)-Methyl-3-(4-(((3-hydroxy-2-methyl-6-(3,5,12-trihydroxy-3-(2-hydroxyacetyl)−10-methoxy-6,11-dioxo-1,2,3,4,6,11-hexahydrotetracen-1-yl)oxy)tetrahydro-2 H-pyran-4-yl)amino)methyl)phenyl)−1-methyltriaz-2-ene-1-carboxylate (**doxorubizen**) was synthesized from doxorubicin (50 mg) and purified by silica gel column chromatography. [MeOH: DCM (2: 8), v/v]; yield: 42 mg (62%), R_f= 0.66, red solid[1];H NMR (400 MHz, $CDCl_3$): δ (ppm) 8.02 (d, *J* = 7.6 Hz, 1 H), 7.78 (t, *J* = 8.1 Hz, 1 H), 7.52 (d, *J* = 8.1 Hz, H), 7.39 (d, *J* = 8.3 Hz, 1 H), 7.31 (d, *J* = 8.2 Hz, 2 H), 5.53 (br. s, 1 H), 5.31 (br. s, 1 H), 4.75 (s, 2 H), 4.69 (br. s., 1 H), 4.08(s, 3 H), 3.97 (m, 1 H), 3.95 (s, 3 H), 3.85 (d, *J* = 13.2 Hz, 1 H), 3.76 (d, *J* = 13.1 Hz, 1 H), 3.68 (br. s., 1 H), 3.43 (s, 3 H), 3.25 (m, 1 H), 3.03–2.94 (m, 2 H), 2.36 (d, *J* = 14.8 Hz, 1 H), 2.15 (d, *J* = 14.5 Hz, 1 H), 1.85 (m, 1 H), 1.71 (d, *J* = 13.4 Hz, 1 H), 1.37 (d, *J*= 6.5 Hz, 3 H)[13];C NMR (100 MHz, $CDCl_3$): δ (ppm) 213.9, 187.2, 186.9, 161.2, 156.3, 155.8, 155.1, 148.3, 135.9, 135.6, 133.9, 133.7, 129.0, 122.5, 121.0, 120.0, 118.6, 111.7, 100.9, 69.5, 67.0, 66.9, 65.6, 56.8, 54.2, 52.6, 49.9, 35.6, 34.1, 30.4, 30.1, 17.3. HRMS (ESI) m/z: calcd for $C_{37}H_{40}N_4O_{13}$ $[M+H]^+$: 749.2670, found: 749.2670.

(S, Z)-Methyl3-(4-(((4,11-diethyl-4-hydroxy-3,14-dioxo-3,4,12,14-tetrahydro-1 H pyrano [3',4':6,7] indolizino[1,2-b]quinolin-9-yl)oxy)methyl)phenyl)−1-methyltriaz-2-ene-1-carboxylate (**1**): The compound was synthesized from SN-38 (50 mg) and purified by silica gel column chromatography [MeOH: DCM (1:9), v/v]; yield: 59 mg (78%), R_f= 0.74, Brown solid[1];H NMR (400 MHz, $CDCl_3$) δ (ppm): 8.13 (d, *J* = 9.2 Hz, 1 H), 7.67 (s, 3 H), 7.60 (s, 4 H), 7.64 (s, 3 H), 7.54 (d, *J* = 8.3 Hz, 7 H), 7.48 (dd, *J* = 2.6, 9.3 Hz, 4 H), 7.30 (d, *J* = 2.4 Hz, 3 H), 5.70 (d, *J* = 16.1 Hz, 3 H), 5.28 (s, 3 H), 5.23 (s, 2 H), 5.15 (s, 2 H), 4.19 (br. s.,

1 H), 3.97 (s, 3 H), 3.96 (d, 1 H), 3.47 (d, 3 H), 3.06 (d, *J* = 7.8 Hz, 2 H), 1.88 (dd, *J* = 7.5, 9.3 Hz, 2 H), 1.32 (t, *J* = 7.6 Hz, 3 H), and 0.99 (t, *J* = 7.4 Hz, 3 H)[13];C NMR (100 MHz, $CDCl_3$) δ(ppm): 174.0, 157.8, 157.7, 155.0, 150.4, 149.8, 148.9, 147.3, 145.5, 143.8, 136.9, 132.3, 128.3, 128.1, 127.4, 122.8, 122.6, 118.0, 103.4, 97.6, 73.0, 70.1, 66.4, 54.3, 49.5, 31.7, 30.4, 23.2, 13.6, and 7.9. HRMS (ESI) m/z: calcd for $C_{32}H_{31}N_5O_7$ $[M+H]^+$: 598.2301, found: 598.2302.

(E)-Methyl-3-(4-(((2-(2,6-dioxopiperidin-3-yl)−1-oxoisoindolin-4-yl)amino) methyl)phenyl)−1-methyltriaz-2-ene-1-carboxylate (**2**): The compound was synthesized from lenalidomide (50 mg) and purified by silica gel column chromatography [ethyl acetate: petroleum ether (6: 4), v/v]; yield: 61 mg (68%), R_f = 0.53, white solid[1];H NMR (400 MHz, CDCl3) δ(ppm): 7.50 (d, *J* = 8.3 Hz, 2 H), 7.40 (d, *J* = 8.3 Hz, 2 H), 7.30 (br. s., 1 H), 7.27–7.21 (m, 1 H), 6.82 (d, *J* = 7.5 Hz, 1 H), 5.19 (dd, *J* = 5.1, 13.3 Hz, 1 H), 5.00–4.85 (m, 2 H), 4.21 (s, 1 H), 4.12–4.09 (s, 1 H), 3.95 (s, 3 H), 3.44 (s, 3 H), 2.95 (m, 1 H), 2.90–2.76 (m, 1 H), 2.30–2.15 (m, 1 H), 2.10 (d, *J* = 5.1 Hz, 1 H)[13];C NMR (100 MHz, $CDCl_3$) δ (ppm): 171.1, 170.2, 169.9, 155.0, 148.4, 141.4, 137.6, 132.4, 129.8, 129.6, 126.3, 122.3, 118.2, 114.4, 54.2, 52.7, 45.1, 43.4, 32.2, 30.4, 22.7. HRMS (ESI) m/z: calcd for $C_{23}H_{24}N_6O_5$ $[M+Na]^+$: 487.1706, found: 487.1709.

(E)-methyl3-(4-((4-((5R,5aR,8aR,9 S)−9-(((2R,4aR,7R,8R,8aS)−7,8-dihydroxy-2-(methylhexahydropyrano[3,2-d][1,3]dioxin-6-yl)oxy)−6-oxo-5,5a,6,8,8a,9-hexahydrofuro-[3',4':6,7] naphtho[2,3-d][1,3]dioxol-5-yl)−2,6-dimethoxyphenoxy) methyl)phenyl)−1-methyltriaz-2-ene-1-carboxylate (**3**): The compound was synthesized from Etoposide (50 mg) and purified by silica gel column chromatography [ethyl acetate : petroleum ether (5 : 5), v/v]; yield: 39 mg (58%), R_f = 0.61, white Solid[1];H NMR (400 MHz, $CDCl_3$) δ (ppm): 7.64 (d, J = 8.3 Hz, 2 H), 7.55(d, J = 8.3 Hz, 2 H), 6.80 (s, 1 H), 6.44 (s, 2 H), 6.24 (s, 1 H), 6.01–5.92 (s, 2 H), 5.06 (s, 2 H), 4.93 (d, *J* = 3.1 Hz, 1 H), 4.72 (d, *J* = 5.0 Hz, 1 H), 4.65–4.58 (m, 1 H), 4.56–4.37 (m, 2 H), 4.25 (d, *J* = 4.9 Hz, 1 H), 4.16 (dd, *J* = 5.0, 10.3 Hz, 2 H), 3.98 (s, 73 H), 3.96 (d, *J* = 7.6 Hz, 1 H), 3.79 (s, 6 H), 3.71 (s, 3 H), 3.62–3.53 (m, 2 H), 3.48 (m, 3 H), 3.46–3.41 (m, 2 H), 3.35–3.26 (m, 2 H), 3.22 (dd, *J* = 5.0, 9.8 Hz, 1 H), 3.15 (dd, *J* = 4.8, 9.7 Hz, 1 H), 3.02–2.95 (m, 1 H), 2.90–2.85 (m, 1 H), 1.36 (d, *J* = 5.0 Hz, 3 H)[13];C NMR (100 MHz, $CDCl_3$) δ (ppm) 180.5, 155.2, 153.9, 152.9, 148.7, 146.5, 138.9, 136.0, 133.2, 129.2, 126.2, 122.1, 109.8, 108.6, 106.1, 101.5, 99.8, 79.9, 75.5, 74.6, 74.6, 73.2, 69.6, 66.6, 56.4, 54.2, 44.4, 44.2, 39.6, 30.3, 20.4; HRMS (ESI) m/z: calcd for $C_{39}H_{43}N_3O_{15}$ $[M+H]^+$: 794.2772, found: 794.2769; or $C_{39}H_{43}N_3O_{15}$ $[M+Na]^+$: 816.2592, found: 816.2594.

(E)-methyl3-(4-((2-methoxy-5-((Z)−3,4,5-trimethoxystyryl) phenoxy)methyl) phenyl)−1-methyltriaz-2-ene-1-carboxylate (**4**): The compound was synthesized from combretastatin (50 mg) and purified by silica gel column chromatography [ethyl acetate : petroleum ether (2 : 8), v/v]; yield: 69 mg (84%), R_f = 0.65, white solid[1];H NMR (400 MHz, $CDCl_3$) δ (ppm): 7.58 (d, *J* = 8.6 Hz, 2 H), 7.37 (d, *J* = 8.6 Hz, 2 H), 6.86 (d, *J* = 12 Hz, 1 H), 6.8 (d, *J* = 12 Hz, 1 H), 6.50 (s, 2 H), 6.44 (d, *J* = 1.6 Hz, 2 H), 4.97 (s, 2 H), 3.98 (s, 3 H), 3.88 (s, 3 H), 3.85 (s, 3 H), 3.71 (s, 3 H), 3.48 (s, 3 H)[13];C NMR (100 MHz, $CDCl_3$) δ (ppm): 155.1, 153.1, 149.1, 148.5, 147.6, 137.9, 137.2, 133.2, 129.9, 129.7, 129.0, 128.0, 122.8, 122.4, 114.7, 111.6, 106.1, 70.6, 61.1, 56.1, 56.1, 54.2, 30.7; HRMS (ESI) m/z: calcd for $C_{28}H_{31}N_3O_7$ $[M+Na]^+$: 544.2060, found: 544.2065.

(E)-methyl3-(4-((5-fluoro-2,4-dioxo-3,4-dihydropyrimidin-1(2 H)-yl)methyl) phenyl)−1-methyltriaz-2-ene-1-carboxylate (***5***): The compound was synthesized from 5-fluorouracil (50 mg) and purified by silica gel column chromatography [ethyl acetate : petroleum ether (4 :6), v/v]; yield: 82 mg (64%), R_f = 0.71, white Solid[1];H NMR (400 MHz, $CDCl_3$) δ (ppm): 7.63 (d, *J* = 8.44 Hz, 11 H)· 7.34 (d, *J* = 8.56 Hz, 12 H), 7.20 (s, 1 H), 4.91 (s, 2 H), 3.97 (s, 3 H), 3.47 (s, 3 H)[13];C NMR (100 MHz, $CDCl_3$) δ (ppm): 155.0, 150.3, 149.3, 148.7, 136.8, 135.1, 130.2, 129.2, 123.1, 122.4, 54.4, 52.2, 30.4; HRMS (ESI) m/z: calcd for $C_{14}H_{14}FN_5O_4$ $[M+Na]^+$: 358.0927, found: 358.0930.

(E)-Methyl 3-(4-(((7 H-purin-6-yl)thio)methyl)phenyl)−1-methyltriaz-2-ene-1-carboxylate (**6**): The compound was synthesized from 6-mercaptopurine (50 mg) and purified by silica gel column chromatography [ethyl acetate: petroleum ether (5: 5), v/v]; yield: 104 mg (89%), R_f = 0.72, light yellow solid[1]. H NMR (400 MHz, DMSO-d_6): δ (ppm): 8.74 (s, 1 H), 8.45 (s, 1 H), 7.58 (d, J = 8.6 Hz, 2 H), 7.49 (d, *J* = 8.4 Hz, 2 H), 4.70 (s, 2 H), 3.88 (s, 3 H), 3.36 (s, 3 H)[13];C NMR (DMSO-d_6, 100 MHz): δ (ppm): 154.1, 151.4, 147.3, 138.9, 130.0, 121.8, 121.8, 54.0, 31.2, 30; HRMS (ESI) m/z: calcd for $C_{15}H_{15}N_7O_2S$ $[M+Na]^+$: 380.0906, found: 380.0909.

(E)-methyl1-methyl-3-(4-(((6-(trifluoromethoxy)benzo[d]thiazol2yl)amino)methyl) phenyl) triaz-2-ene-1-carboxylate (**7**): The compound was synthesized from Riluzole (50 mg) and purified by silica gel column chromatography [ethyl acetate: petroleum ether (6: 4), v/v]; yield: 67 mg (72%), R_f = 0.61; white solid[1]:H NMR (400 MHz, $CDCl_3$) δ (ppm): 7.41 (d, J = 8.3 Hz, 2 H), 7.25 (d, J = 8.3 Hz, 2 H) 7.22 (m, 1 H), 7.18 (d, *J* = 8.8 Hz, 1 H), 6.93 (d, *J* = 7.9 Hz, 1 H), 4.46 (s, 2 H), 3.78 (s, 3 H), 3.28 (s, 3 H)[13];C NMR (100 MHz, $CDCl_3$) δ (ppm): 168.2, 155.1, 151.0, 148.7, 143.8, 137.9, 131.1, 128.5, 122.7, 119.9, 119.2, 114.2, 54.2, 49.1, 30.4; HRMS (ESI) m/z: calcd for $C_{18}H_{16}F_3N_5O_3S$ $[M+H]^+$: 440.1004, found: 440.1004.

Cell culture

The human B-cell leukemia cell lines MUTZ5 and MHH-CALL4, the T-cell leukemia cell line DND41, and the erythroleukemic HEL were kindly provided by Prof. Shai Izraeli (Schneider Children's Medical Center, Petach Tikvah, Israel). BV-173 cells were obtained from DSMZ (cat #: ACC 20). The human mantle cell lymphoma cell lines Jeko-1, Mino, and Rec-1 were purchased from ATCC. The above cells were cultured in RPMI medium (Gibco, Thermo Fisher Scientific, Inc., USA). Granta cells were kindly provided by Prof. Martin Dreyling (University of Munich, Munich, Germany) and were grown in

Dulbecco's Modified Eagle Medium (DMEM, Gibco, Thermo Fisher Scientific, Inc., USA). OCI-AML3 and KG-1a cells were kindly provided by Dr. Liran Shlush (Weizmann Institute, Rehovot, Israel) and were grown in Iscove's Modified Dulbecco's Medium (IMDM, Gibco, Thermo Fisher Scientific, Inc., USA). All media were supplemented with 10% heat-inactivated fetal bovine serum (FBS; Biological Industries, Israel), 2 mM glutamine (Biological Industries, Israel) and 1% penicillin and streptomycin (Biological Industries, Israel). The cells were cultured at 37 °C in a humidified incubator with 5% CO_2.

In vitro cytotoxicity assay

Growth inhibition in hematological malignancy cell lines was measured by a tetrazolium WST-1 assay (Roche, Basel, Switzerland). Cells (1×10^4) were treated with various concentrations of the specific chimera or parental drug. After 48 h of incubation, 10 µl of WST-1 reagent was added to the plate and incubated for 1 h at 37 °C, at which point the absorbance (450 nm) was measured in an ELISA plate reader (Synergy HTX multimode reader, Winooski, Vermont, USA).

Mitochondrial depolarization

Changes in the mitochondrial potential and cellular plasma membrane permeabilization were determined with the Muse® Mitochondrial Kit (Luminex, USA). Briefly, cells were treated with DMSO or the relevant chimera for 48 h. The cells were incubated with a MitoPotential working solution for 20 min at 37 °C in 5% CO_2. Then, 5 µL of Muse® MitoPotential 7-ADD reagent was added, and the cells were incubated for 5 min at room temperature. The percentages of four cell populations, live (mitopotential+/7-AAD−), depolarized live (mitopotential−/7-AAD−), dead (mitopotential+/7-AAD+), and depolarized dead (mitopotential−/7-AAD+), were measured using a Muse® Cell Analyzer (Luminex, USA).

Apoptosis assay

The cells were analyzed using the multifunctional Muse® Annexin V and Dead Cell Kit (Luminex/Millipore, Austin, Texas, USA). The cells were treated with the indicated drugs or chimeras. After 48 h of incubation, the cells were harvested, washed twice in PBS, and 2×10^5 cells were stained with 100 µl of Muse Annexin V and Dead Cell Reagent. The samples were incubated for 20 min at room temperature in the dark. The cells were analyzed with a Muse® Cell Analyzer system (Millipore, Billerica, MA, USA), and the percentage of apoptotic cells was determined using Guava software (Luminex/Millipore, USA, version 3.3).

DNA damage quantitation by dual staining at pH 2 A. X and pATM

BV-173 cells (2×10^5 cells/well) were treated with DMSO, doxorubicin, or **doxorubizen**. After incubating for 2 h, the phosphorylation levels of ATM and H2AX were measured via a Muse cell analyzer using the Muse Multi-Color DNA Damage Kit (Luminex Corporation, Part number: MCH200107) according to the manufacturer's instructions. Phosphorylation levels were determined using Guava software (Luminex/Millipore, USA, version 3.3).

Hydrolytic stability studies

Solutions of **doxorubizen**(0.075 mg/ml) in acetate buffer at pH 4.6, pH 5.3, PBS at pH 7.4 and phosphate buffer at pH 8.0 were filtered and incubated at 37 °C. The buffers were prepared following standard procedures[32]. At the indicated time points, an aliquot was collected and analyzed via LC-UV/MS (λ = 290 nm). Compound peaks were integrated and compared to the integration at t0 to calculate the percentage of prodrug remaining.

DNA intercalation assay (DNA/methyl green colorimetric assay)

The affinity of the **doxorubizen** for DNA binding was examined in vitro using a DNA/methyl green assay with doxorubicin as a positive control. In this test, a mixture of methyl green (20 mg) (Merck) and calf thymus DNA (10 mg) (Merck) was suspended in 0.05 M Tris HCl buffer (100 mL, pH 7.5) containing 7.5 mM $MgSO_4$. This mixture was stirred continuously for 24 h at 37 °C. Then, ethanolic solutions of the test compounds were added to the wells of a 96-well microtiter tray at concentrations of 10, 100 and 1000 µM. The excess solvent was removed from each well under vacuum, after which 200 µL of the DNA/methyl green solution was added. The test samples were incubated for 24 h in the dark at ambient temperature. After that, the absorbance of each sample was determined at 642.5–645 nm. The IC_{50}values were determined by linear regression of the data plotted on a semilog scale, and the data were compared with those obtained with doxorubicin as a standard DNA intercalator[46], 47.

Topoisomerase IIα supercoiled plasmid DNA relaxation assay

The Topo IIα activity inhibition assay was performed using a Topoisomerase II drug screening kit according to the manufacturer's instructions (TopoGEN, Buena Vista, CO). In brief, Dox and **doxorubizen** were diluted in 10 mM Tris buffer (pH 8) supplemented with 1% DMSO to final concentrations of 0.05, 0.1, 1, and 10 µM. Dox and **doxorubizen** were incubated with 250 ng of pHOT plasmid and 2 units of Topo IIα for 30 min at 37 °C. DMSO (1%) served as the solvent control. The reaction was terminated by the addition of 2 µL of 10% SDS followed by 15 min of incubation at 37 °C with 50 ng/ml proteinase K. The reaction products were analyzed using a 1% agarose gel in the absence of ethidium bromide. After

electrophoresis separation, the gel was stained with 0.5 µg/ml ethidium bromide for 15 min and destained for 10 min in water[46].

Receptor and ligand Preparation

The crystal structures of the human TOPO IIβ-DNA complex and its ligand etoposide were retrieved from the PDB[36]database (PDB code: 3QX3)[37]. The structure (chain A) was used for docking the co-crystallized ligand etoposide and the two other compounds doxorubicin and **doxorubizen**(chimera). The protein and the co-crystallized ligand were prepared using the Schrödinger Maestro[38]protein preparation wizard protocol using default parameters. The ligand was deleted from the prepared protein structure prior to docking. The other ligands were prepared using the "ligprep" panel with Epik[39]tool, using OPLS4 force field at pH value (7.0 ± 2.0), and subjected to a conformational search using the "Generate conformations" protocol. Docking of these conformations into TOPO IIβ-DNA was carried out using Glide[40] XP protocol with default settings. The pose with the best docking score was selected.

MD simulation

The molecular dynamics simulations were carried out using the Desmond simulation package of Schrödinger LLC. The system was constructed with an SPC[44] solvent model. The *NPT* ensemble with a pressure of 1 bar and a temperature of 300 K was applied in all runs. The simulation length was 100 ns, with 1000 frames for the **doxorubizen**/TOPO IIβ complex. The OPLS4 force field parameters were used in all the simulations. The Martyna – Tobias – Klein chain coupling scheme with a coupling constant of 2.0 ps was used for pressure control, and the Nose´- Hoover chain coupling scheme[45] was used for temperature control.

MM/GBSA

Prime MM/GBSA[41]calculations were performed to determine the free binding energy (ΔG) of the complexes using the hierarchical sampling algorithm to obtain accurate positions of protein residues and ligand functional groups. The calculations were performed using the OPLS4[42]force field and the VSGB 2.0 solvation model[43].

BV-173 leukemia xenotransplantation model and in vivo preclinical studies

All animal experimental protocols were approved by the Institutional Animal Care and Use Committee of Tel-Aviv University, Israel (permit # TAU - MD - IL – 2307 – 152–5) and were performed in accordance with ARRIVE guidelines. NOD-SCID IL2Rgnull (NSG) mice were obtained from The Jackson Laboratory. Mice were housed within the Tel Aviv University Specific Pathogen Free (SPF) facility in individually ventilated cages with four to five animals of the same sex per cage. All mice were maintained on a regular diurnal lighting cycle (12:12 light: dark) with ad libitum access to food and water. BV-173 cells (1×10^6 cells/animal) were resuspended in saline and transplanted via tail vein (final volume of 0.2 ml/animal) into 8- to 12-week-old female NSG mice. Treatments were initiated 12 days post-transplantation. All the drugs were dissolved first in DMSO to obtain a 50 mM stock solution. Drugs in DMSO were further diluted in saline to obtain a 5.6% solution (v/v) of solvent for injection. Mice were randomly assigned to the experimental groups. They received equimolar concentrations of doxorubicin (1.2 mg/kg), **doxorubizen** (1.68 mg/kg), or solvent intraperitoneally (final volume of 25 µl/animal) for three consecutive days. The animals were weighed prior to treatment, and the doses were recalculated to ensure that the mice received a consistent dose of the drugs. Tail vein and intraperitoneal injections were performed without anesthesia. To ensure humane endpoints, mice were monitored daily for health parameters according to the protocol approved by the Institutional Animal Care and Use Committee of Tel-Aviv University (TAU - MD - IL – 2307 – 152–5). Changes in any of the following parameters were defined as a human endpoint: body weight loss of 20% or more between the measurements (monitored by laboratory balances), lethargy, ruffled fur, hind limb paralysis, hunched posture and labored breathing (all monitored by visual inspection). Upon meeting the humane endpoint criteria or twenty days after the last injection, mice were euthanized by CO2 inhalation using a fill rate of 50% of the chamber volume/minute. CO2 flow was maintained for at least 2 min after breathing stops to ensure death. Euthanasia was confirmed by the absence of breathing and reflexes. No secondary method of euthanasia was performed. Human engraftment in the bone marrow and spleen was analyzed by flow cytometry using human-specific CD45-PC7 (Beckman Coulter) and CD33-PE (BioLegend) antibodies.

Statistical analysis

All studies were performed at least 3 times unless otherwise stated. The data are presented as the means ± standard deviations, and the statistical significance of the differences was determined using unpaired two-tailed Student's t tests (GraphPad Prism), with a p-value < 0.05 indicating statistical significance.

All methods were performed in accordance in accordance with The TRUST Code recommendations.

Results

One-pot synthesis of chimeras

In our research, the main requirement for drugs to form chimeras was the presence of free functional groups, such as amines, hydroxy groups, and thiols, suitable for alkylation reactions with **azene**bromide[14]. The parent drugs SN-38, lenalidomide, etoposide, bretastin, 5-fluorouracil, 6-mercaptopurine, riluzole,

and doxorubicin are equipped with such functionalities, enabling the synthesis of corresponding chimeras **1–7** and **doxorubizen** by alkylation with the previously employed **azene** bromide tether. The resulting chimeras were prepared in good yields, as shown in Fig. 1A. Notably, **azene** bromide, similar to **azene**, is protected by a biolabile methyl carbamate group at the monomethyl triazene segment, which is bound through the self-immolative 4-aminobenzyl linker. After testing several reaction conditions, we found that the alkylation of all the above-mentioned drugs was optimal when 1 equiv. of **azene** bromide was used with 1.2 equiv. of K_2CO_3 in DMF at room temperature for 12 h under N_2. Pure products were obtained after flash chromatography on silica gel using ethyl acetate/petroleum ether or DCM/MeOH gradients in good yields (58–89%), and their structures were confirmed by ^{1}H NMR[13], C NMR, and HRMS.

In vitro cytotoxicity screening of chimeras

We explored the cytotoxic effects of the newly synthesized chimeras **1–7** and **doxorubizen** on ten hematological cell lines representing different disease models: Granta, Rec-1, Mino, and Jeko-1 for the mantle cell lymphoma (MCL) model; MUTZ5 and MHH-CALL4 for the B-cell acute lymphocytic leukemia (B-cell ALL) model; DND41 for the T-cell ALL model; KG-1a and OCI-AML-3 for the acute myeloid leukemia (AML) model; and HEL for the erythroleukemia model.

Compound screening assays for drug sensitivity are typically conducted at concentrations ranging from 0 to 10 μM[29]. Therefore, we screened our newly synthesized compounds in this range. Among all the chimeras, **doxorubizen** exhibited significant proliferation inhibition at a low dose of 50 nM. Consequently, we compared the cytotoxic effect of **doxorubizen** to that of the paired substrate doxorubicin. We focused on the four most aggressive hematological malignancy cell lines (Granta, Jeko-1, KG-1a, and OCI-AML3) and assessed the impact of **doxorubizen** vs. Dox on an additional aggressive cell line, BV-173. This cell-line is derived from a patient with Philadelphia chromosome-positive B-cell acute lymphoblastic leukemia (Ph + B-ALL), which is characterized by the BCR-ABL1 fusion gene, a hallmark of aggressive leukemia with high relapse rates. It is widely used as a preclinical model to study the biology of Ph + leukemias and to evaluate novel therapeutic agents due to its high proliferation rate, leukemogenic potential in xenograft models, and responsiveness to anti-leukemia therapies. Treatment with 50 nM **doxorubizen** significantly reduced the proliferation rate of all the tested cell lines compared with that of the parental drug doxorubicin (Fig. 1B). The 50% inhibitory concentrations (IC_{50}s) of doxorubizen and Dox in the tested cell lines are presented in Table S2.

Doxorubizen induces mitochondrial depolarization, apoptosis and cell death

Mitochondrial membrane potential depolarization prevents calcium entry into mitochondria. This is a critical step in the progression to cell death. Doxorubicin causes changes in mitochondrial redox potentials, leading to depolarization, which is associated with cell cycle arrest and cell death[30]. We evaluated the biological impact of **doxorubizen** on mitochondrial function and cell death compared to that of Dox. To that end, we treated BV-173, Granta, Jeko-1, KG-1a, and OCI-AML3 cells with Dox or **doxorubizen** at a concentration of 50 nM. The results are demonstrated in Fig. 2. Treatment with **doxorubizen** led to a significant decrease of the mitochondrial membrane potential in the treated cells. Furthermore, there was a substantial increase in the rate of apoptosis compared to that in cells treated with the parental drug Dox or untreated cells (Fig. 3) across all the tested cell lines.

Doxorubizen induces more DNA damage than does the parental drug

Due to two factors, namely, their high in vitro sensitivity to both the parental drug and **doxorubizen** at 50 nM and the availability of a BV-173 cell line xenograft model in our laboratory, we concentrated on BV-173 cells to better understand the biological mechanism of **doxorubizen**. Cells were treated with Dox or **doxorubizen**, and DNA damage was analyzed after 2 h by dual staining for phospho-histone H2A. X (Ser139) and phospho-ATM (Ser1981) antibodies. We observed significant coactivation of pH2A. X and pATM upon treatment with **doxorubizen** (Fig. 4A). Additionally, a recent study suggested that loss of p53-binding protein 1 (53BP1) reduces the survival of cancer cells following DNA damage caused by radiotherapy treatment[31]. Therefore, we examined 53BP1 protein expression levels in BV-173 cells following treatment with **doxorubizen** and found a significant decrease in protein levels (Fig. 4B-C). Moreover, we observed elevated protein levels of the tumor suppressor gene TP53 following treatment with **doxorubizen** (Fig. 4B-C), indicating that compared with the parental drug Dox, **doxorubizen** induced substantial DNA damage and double-strand breaks in treated cells.

Hydrolytic stability of doxorubizen

The purpose of the stability experiments described here was to estimate the stability/decomposition rate of **doxorubizen** at physiological pH (7.4 in PBS) and pH across different organelles, which can span within the range of 4.5 to 8.0 (see Fig. 5A). We observed **doxorubizen** to be significantly stable at a physiological pH of 7.4 and an acidic pH of 5.3, with approximate $t_{1/2}$ values of 2 d and 8 d, respectively, as evidenced by LCMS monitoring (see Fig. 5B). Both the hydrolytic lysosomal pH 4.6 and the more basic medium (pH 8) **doxorubizen** was less stable ($t_{1/2}$of approximately 18 h), though it still exhibited respectable stability. Notably, the drug TMZ, which also bears a monomethyl triazene moiety, is spontaneously hydrolyzed in aqueous solution (pH 7.4) and has a half-life of ~1.5–2 h[32]. These results support our hypothesis that

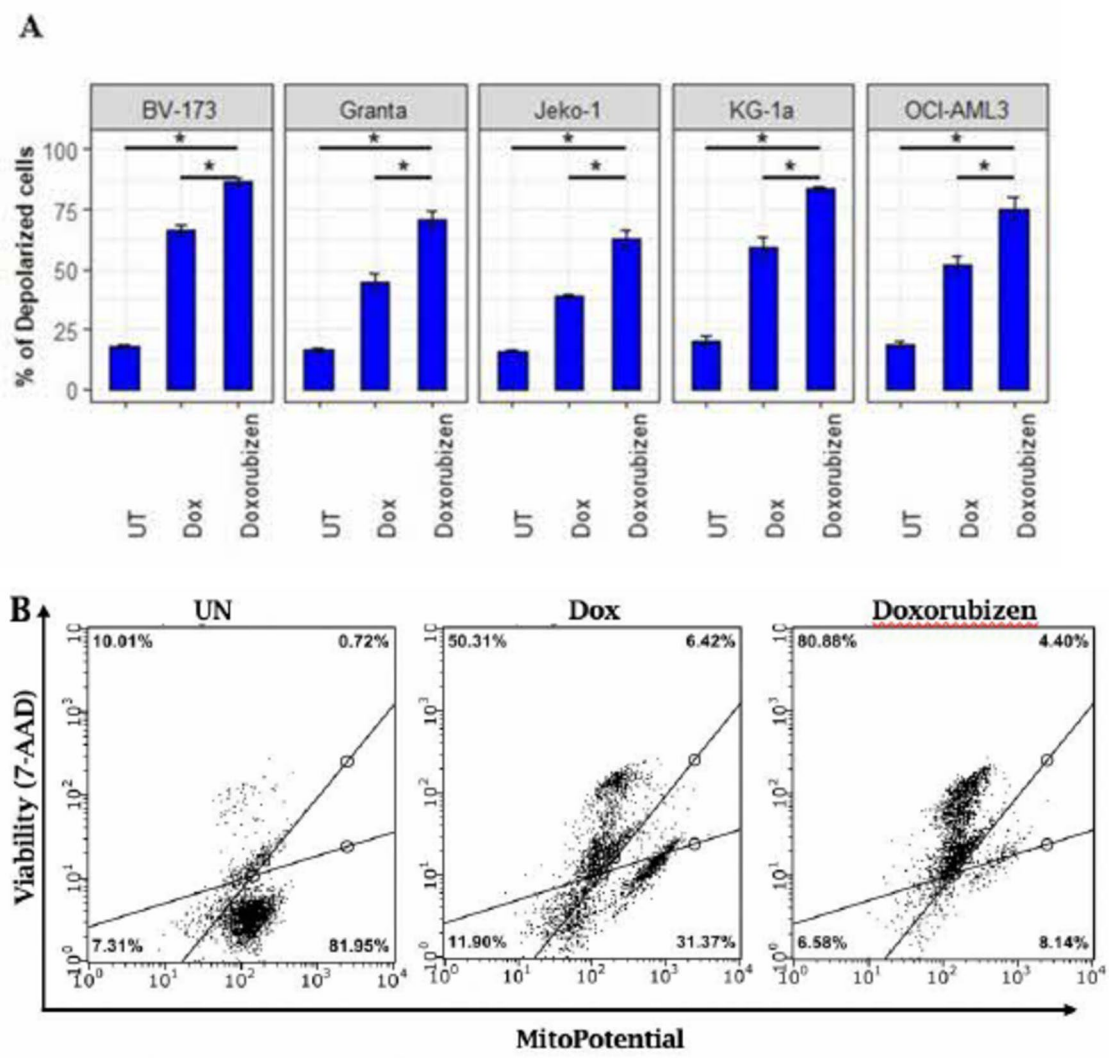

Fig. 2. Treatment with Doxorubizen induces mitochondrial membrane potential depolarization. A. The percentage of the depolarized cell population in BV-173, Granta, Jeko-1, KG-1a, and OCI-AML3 cells was measured by the Muse® Cell Analyzer following 48 h of treatment with dox or **doxorubizen** (50 nM each). The graphs represent the means of the total depolarized cells ± SEMs from at least 3 experiments. (*$p < 0.05$). **B**. Representative mitochondrial membrane potential analysis of BV-173 exposed to indicated treatments. Quadrants represent the percentage of four cell populations, live (mitopotential+/7-AAD−), depolarized live (mitopotential−/7-AAD−), dead (mitopotential+/7-AAD+), and depolarized dead (mitopotential−/7-AAD+), as measured by a Muse® Cell Analyzer. Similar gating strategy and analysis was utilized also for Granta, Jeko-1, KG-1a and OCI-AML3 cell lines following 48 h of treatment with doxorubicin (Dox) or **doxorubizen**. UT: untreated.

doxorubizen acts as a single entity prior to reaching tumoral DNA, followed by compound hydrolysis and methylation of closely located nucleotides.

Molecular Docking and MD simulation of doxorubizen

A docking study was conducted for doxorubicin (Dox) and **doxorubizen** (chimera) compounds. Dox, a potent DNA intercalator, was used as a reference standard. Table 1 represents the calculated binding energies of the compounds. The reliability of the Glide docking procedure was demonstrated by its ability to reproduce the crystallographic ligand pose in the crystal structure of Topo IIβ with an RMSD of 0.63 Å. The resulting docking conformations of **doxorubizen** were subjected to MD simulations using the Desmond package to check the reliability of the docking studies. The best scored docking conformer of **doxorubizen** showed smaller rmsd variations (RMSD = 1.5 Å) than did the other conformations in a 100 ns MD simulation (RMSD > 4.0 Å) (Fig. S29). Smaller rmsd variations indicate the stability of the ligand conformation in that binding pocket throughout the entire simulation. Thus, in accordance with the molecular docking results, the binding site shown (Fig. 6c) for **doxorubizen** is preferable. To

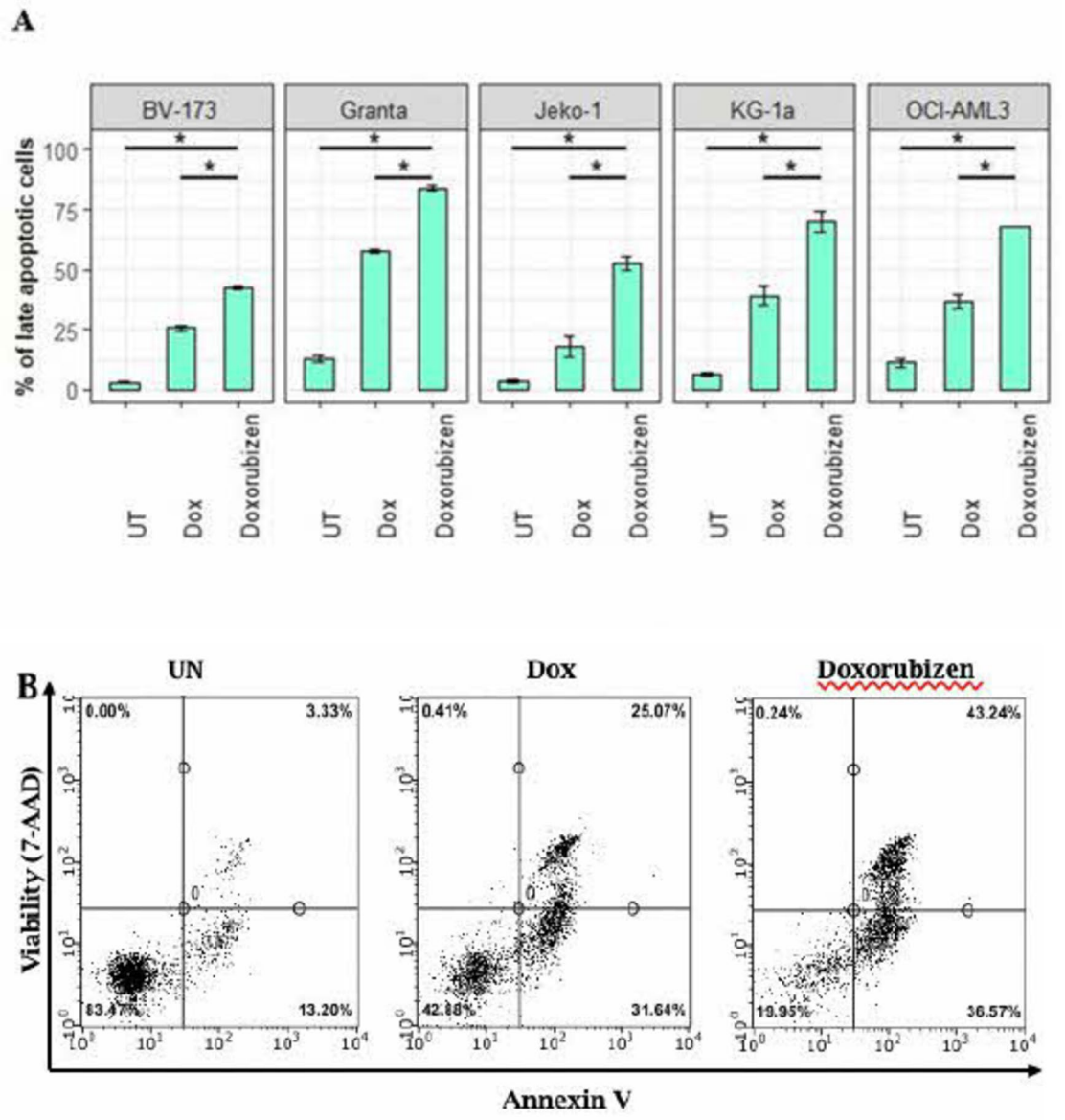

Fig. 3. **Treatment with doxorubizen induces cell apoptosis** The cells were stained with Annexin V and 7AAD, followed by Muse® Cell Analyzer analysis. **A**. The histograms represent the mean number of apoptotic cells (annexin V-positive cells) ± SEM from at least 3 experiments following 48 h of treatment with **doxorubizen** or dox (50 nM each) compared to the untreated cells; $^{*}p < 0.05$. SEM: standard error of the mean. UT: untreated. **B**. Representative apoptosis analysis of BV-173 cells exposed to indicated treatments. The lower left quadrant represents the percentage of viable cells (negative for Annexin and 7AAD), the upper left quadrant represents necrotic cells (7AAD positive, annexin negative), the lower right quadrant represents cells in early apoptosis (annexin positive, 7AAD negative), and the upper right quadrant represents cells that are in late apoptosis (annexin and 7AAD positive). Similar gating strategy and analysis was utilized for the additional cell lines.

specify the nature of the protein–ligand interactions, molecular mechanics/Generalized Born surface area (MM/GBSA) binding energy calculations were carried out using docking conformations as well as MD simulation trajectories (Table 1, Fig. S29). From binding mode analysis, we can see that both Dox and **doxorubizen** are DNA intercalators, as their planar aromatic moieties are positioned within the binding site of Topo II in proximity to four DNA bases (DC8 -C strand, DT9 -D strand, DA12 and DG13 -F strand; Fig. 6a). These binding interactions revealed that Dox can bind to key nucleobases and amino acids of the DNA-Topo II complex protein (Table S1; detailed interactions, Fig. S29) and act as a Topo II inhibitor. Its amino sugar moiety indicates the minor groove binding agent of DNA (Fig. 6b). In contrast, **doxorubizen**exhibits a different binding mode that may result in efficient DNA methylation[33,3]. The two aromatic rings of the tetracene nucleus form π-π stacking interactions with DC8, the C strand and DA12, the F strand base pairs respectively. The C_{12} carbonyl group forms two hydrogen bonds with Arg 503 of

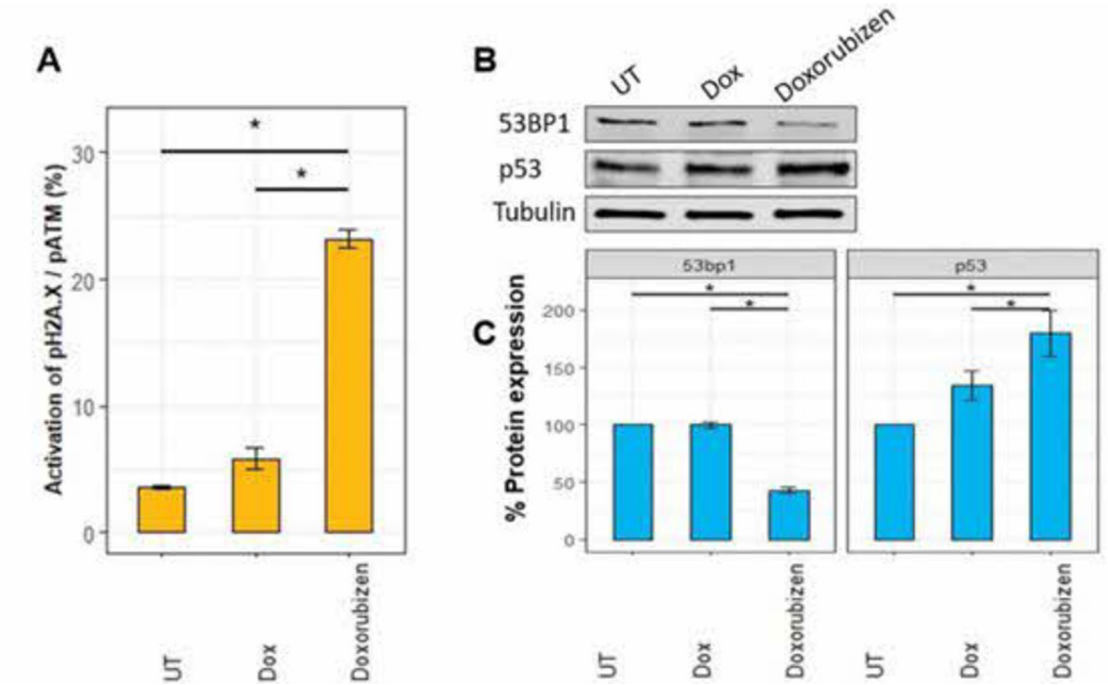

Fig. 4. Induction of DNA damage by doxorubizen in BV-173 leukemic cells. A. Cells were treated with Dox or **doxorubizen** (50 nM each) for 2 h, after which DNA damage was analyzed via dual staining for pH2A.X and pATM. The graph represents the levels of both pH2A.X and pATM as analyzed by the Guava® Muse® Cell Analyzer. **B**. Western blot analysis of 53BP1 and p53 proteins after treatment with Dox (50 nM) or **doxorubizen** (50 nM) for 2 h. Uncropped, full-length gels and blots provided in Figure S31. **C**. Quantification of 53BP1 and P53 mean protein levels ± SEM from at least 3 experiments. Dox or **doxorubizen** were used at 50 nM each. Tubulin was used as a loading control, $*p < 0.05$. UT: untreated.

Topo II. The C_{11} OH and C_{14} OH groups form hydrogen bonds with DG13. The C_9 OH attached to the tetracene nucleus and C_7 O are bound to DA12 via hydrogen bonds. The OH and NH_2 groups attached to pyran ring form H-bond and salt bridge with Ala 816, DC11 phosphate backbone respectively. The adjacent carbonyl group of triazene part forms H-bond with Arg 820 residue of Topo II. These interactions (Fig. 6c) and binding mode revealing **doxorubizen** as a DNA intercalator (Fig. 6d) and Topo II inhibitor. Specifically, tetracene core structure interacts with the DNA base pairs helps positioning the monomethyl triazene part in a favourable orientation that may facilitate methylation at N-7 or C(6) = O nucleophilic center of DG10 guanine base, DNA (Fig. 7). Interestingly, we found that **doxorubizen** is a major groove DNA binding agent (Fig. 2b). The ΔG MM/GBSA results (Table 1) support the biological data and suggest that **doxorubizen** is a stronger Topo II inhibitor than Dox because the ΔG score of **doxorubizen** (−90.71 kcal/mol) is significantly greater than that of Dox (−57.84 kcal/mol).

Displacement of Methyl green from DNA by doxorubizen

In this test, methyl green dye reversibly binds to DNA to form a stable, colored complex of DNA/methyl green at neutral pH. When Dox (positive control) and **doxorubizen** were added, methyl green was displaced from the DNA upon the addition of H_2O to the dye, resulting in the formation of colorless carbinol and leading to a decrease in light absorbance. The ΔA value (the difference between the DNA/methyl green complex and free cabinol) provides a measure for detecting the DNA-binding affinity and relative binding strength. As can be seen in Fig. 8, **Doxorubizen**, with an IC_{50} value of 20 ± 0.43 mM was found to be more potent DNA intercalator than did the parent Dox agent, with an IC_{50}= 44 ± 0.64 mM[46,47].

Doxorubizen inhibits Topo II activity

Binding mode analysis predicted that Dox and **doxorubizen** interact with the Topo II binding site and thus inhibit its activity. We carried out a comparative test to inhibit recombinant human Topo IIα activity in a supercoiled relaxation assay to confirm whether **doxorubizen** exerts its cytotoxicity by inhibiting topoisomerase enzyme activity similarly to Dox [46]. To this end, we incubated the supercoiled pHOT plasmid with DMSO, Dox, or **doxorubizen** (0.05, 0.1, 1, or 10 μM for both drugs) for 30 min at 37 °C. As shown in Fig. 9, both Dox and **doxorubizen** prevented the formation of relaxed plasmid forms in a dose-dependent manner, whereas the supercoiled and linearized products accumulated, which is indicative of

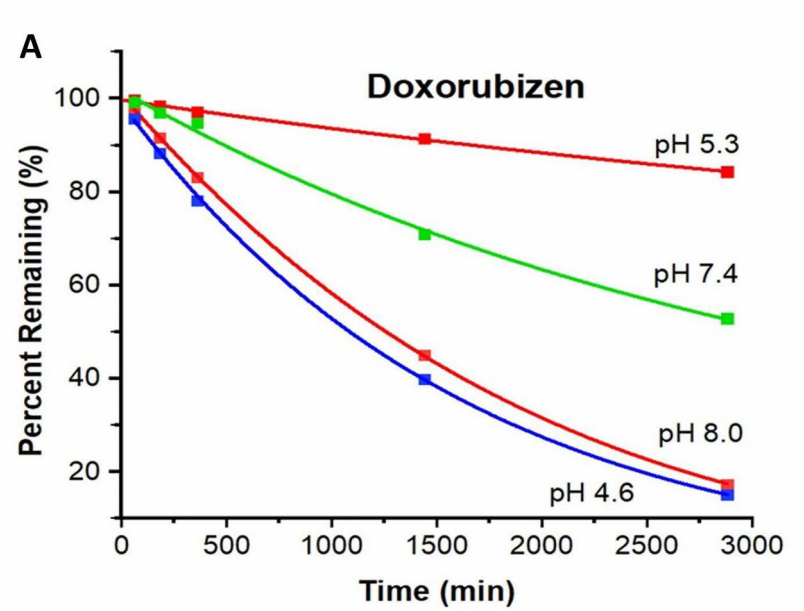

Fig. 5. **(A)** Hydrolytic stability of **doxorubizen** at pH 4.6, 5.3, 7.4, and 8. The percentage of prodrug remaining was quantified by HPLC, n ≥ 2; **(B)** Half-lives of **Doxorubizen** calculated from the hydrolytic stability data.

Ligand	ΔG bind (Kcal/mol)
Doxorubicin	-57.84
Doxorubizen (major conformer)	-90.71

Table 1. Docking results for the two compounds studied in this work together with the crystallized ligand Topo II. Note that a more negative value indicates stronger binders.

Topo II interfacial poisoning. Thus, **azene** modification of Dox results in no interference with the potent inhibitory effects of the parental drug on Topo II.

Doxorubizen reduces leukemia burden in a preclinical leukemia xenograft murine model

To characterize the antileukemic effect of **doxorubizen** in vivo, we utilized a xenograft chemotherapy model. As stated above, we selected the BV-173 leukemia cell line based on its high in vitro sensitivity to both the parental drug and the **doxorubizen** (Figs. 2, 3 and 4) and its ability to achieve uniform multiorgan leukemia engraftment upon intravenous inoculation[34]. Previous studies that model doxorubicin-based chemotherapy doses and delivery in immunodeficient murine strains have demonstrated measurable antileukemia efficacy using a wide dose range (0.25 mg/kg–2.5 mg/kg), a variable number of injections (ranging from 3 to 6 injections), mode of injection (intravenously and intraperitoneally), and intervals between injections (ranging from every day to once a week)[34,35]. Based on the middle-range dose of doxorubicin (1.2 mg/kg), we determined the equimolar dose of **doxorubizen** (1.68 mg/kg) for

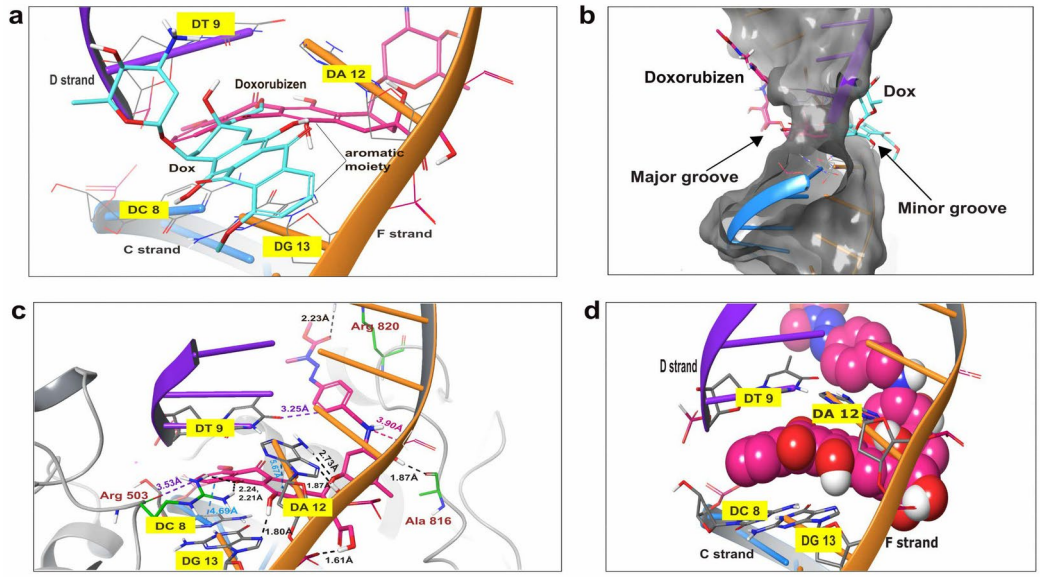

Fig. 6. A. Dox and **doxorubizen** both act as intercalators within the same DNA base pairs. **B.** Dox, DNA minor groove binding agent; **doxorubizen**, DNA major groove binding agent. **C. Doxorubizen** acts as Topo II inhibitor, detailed interactions (hydrogen bond: black; p-p stacking: cyan; aromatic-H bond: violet; salt bridge: pink). **D. Doxorubizen** (space-filling model) acts as intercalator showing between DNA base pairs.

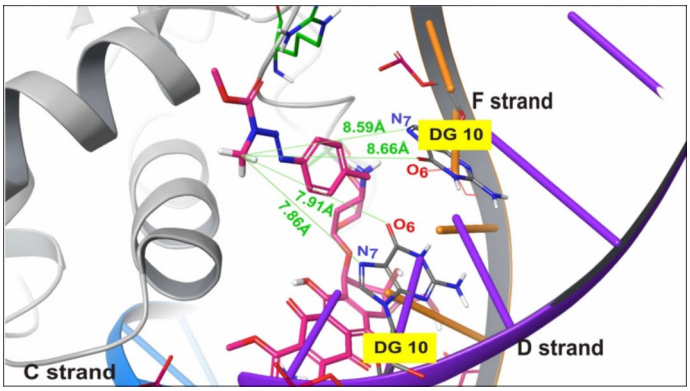

Fig. 7. Representative binding mode of **doxorubizen** in the binding site of Topo II in proximity to the guanine DNA bases DG10. Distances are shown in Å between N7 or O6 of guanine and the monomethyl carbon of triazene. These distances are likely short enough that they may facilitate effective methylation of the guanine bases by **doxorubizen.**

intraperitoneal injection. To establish a more realistic model of leukemia response to chemotherapy, we first allowed mice to develop detectable leukemia engraftment (12 days post-inoculation) and then treated them with three consecutive drug injections (Fig. 10A). We observed progressive weight loss in all the experimental groups starting on day 29 (Fig. 10B), which is indicative of illness; therefore, all the mice were euthanized on day 34 upon reaching the terminal disease stage. Human leukemia engraftment in the bone marrow of the solvent-injected mice was 33.25+/−10.3%. Doxorubicin treatment resulted in a 30% reduction in the leukemia burden relative to that of the solvent (control) (mean 23.3+/−10.3%). Strikingly, an equimolar dose of **doxorubizen** led to a further decrease in leukemia blasts (mean 13.8+/- 9.5%). We also detected a 2.3-fold reduction in the number of leukemic cells infiltrating the spleen (Fig. 10D, E) only in the **doxorubizen**-treated animals, in agreement with the stronger effect of the **doxorubizen** observed in the bone marrow (Fig. 10C, E). Notably, we detected no leukemia cells in 1/5 of the animals in the **doxorubizen**-treated group, suggesting a cure. A previous report indicated liver damage upon intraperitoneal delivery of doxorubicin [35], thus prompting us to compare the effects of both drugs on this organ. We revealed a reduction in liver size indicative of organ damage in all animals treated with doxorubicin, while no gross changes in liver size or shape were detected in the **doxorubizen**-treated group using the same dosing schedule or delivery route (Fig. 10F). Collectively, these data revealed that the novel

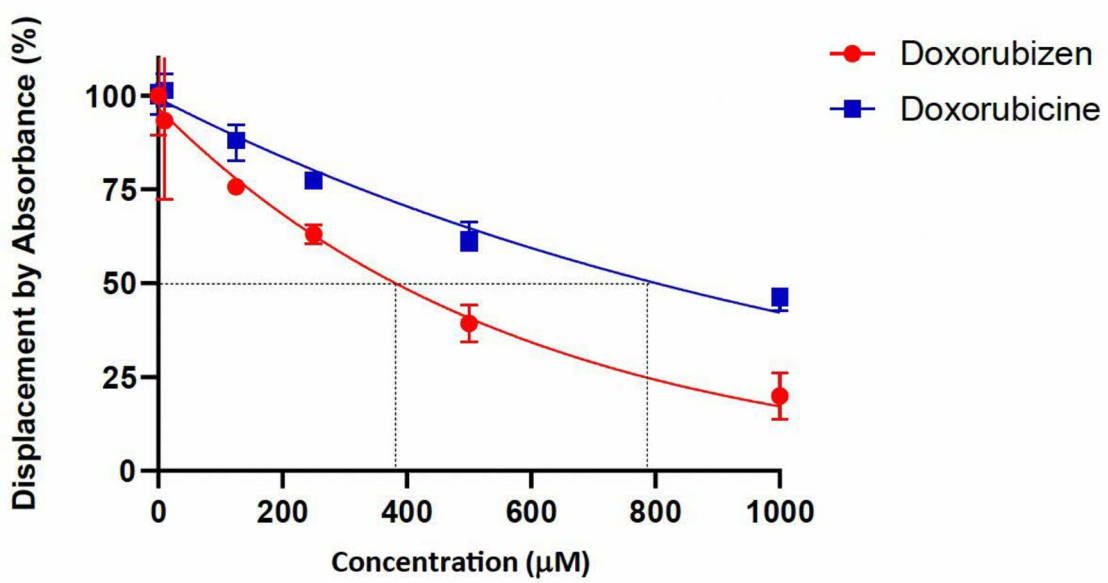

Fig. 8. Displacement of methyl green from DNA by **doxorubizen** and doxorubicin Absorbance readings (mean ± SD, $n = 3$) of solutions of DNA/methyl green in the presence of **doxorubizen** and doxorubicin at the concentrations indicated. The values represent the concentration required for a 50% decrease in the initial absorbance of the DNA methyl green solution.

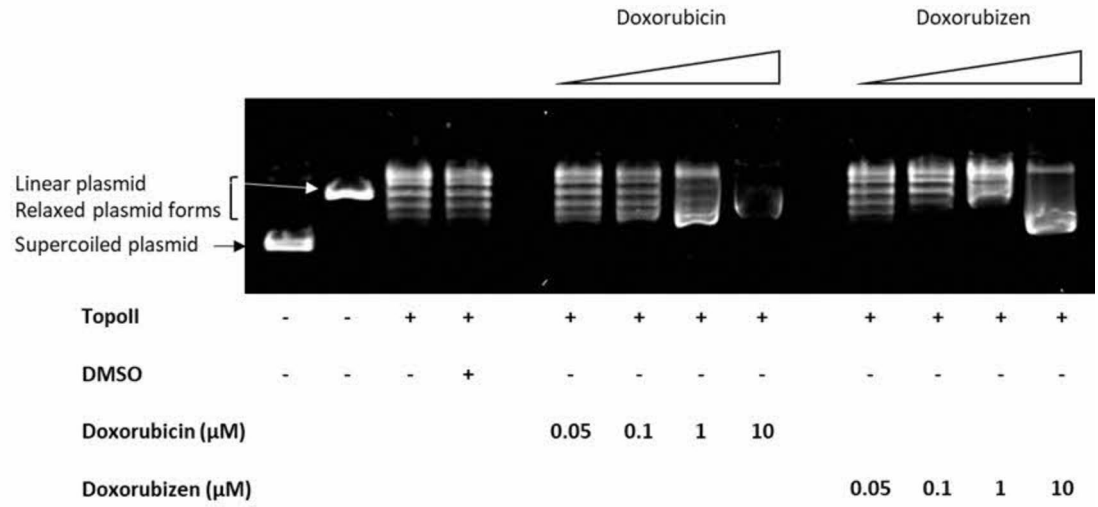

Fig. 9. **Doxorubizen** inhibits Topo II activity. The pHOT plasmid was incubated in the presence of DMSO (solvent control), doxorubicin, or **doxorubizen** (0.05, 0.1, 1, or 10 µM for both drugs) for 30 min at 37 °C. **Doxorubizen** (1 and 10 µM) prevented the formation of relaxed topoisomers, and the linearized pHOT DNA product accumulated.

doxorubicin-based chimera **doxorubizen** elicited significant anti-leukemia activity in vivo and had fewer side effects than its parental drug doxorubicin.

Discussion

In this study, we developed a novel molecular chimera, **doxorubizen**, to enhance the anticancer activities of the known DNA intercalator and Topo II inhibitor drug doxorubicin. **Doxorubizen** operates through two anticancer mechanisms: (1) similar to Dox, it intercalates into DNA to cause DSBs; and (2) it brings the methylating moiety imbedded in methyl triazene to proximity to Topo II-induced DSBs, resulting in effective methylation of DNA. This assumption is supported in silico by resulting MD simulations of the docking conformations of **doxorubizen** and confirmed by DNA intercalation and Topo II inhibition assays. The planar aromatic moieties of Dox and **doxorubizen** are located within the binding site of Topo II, close to four DNA bases, according to

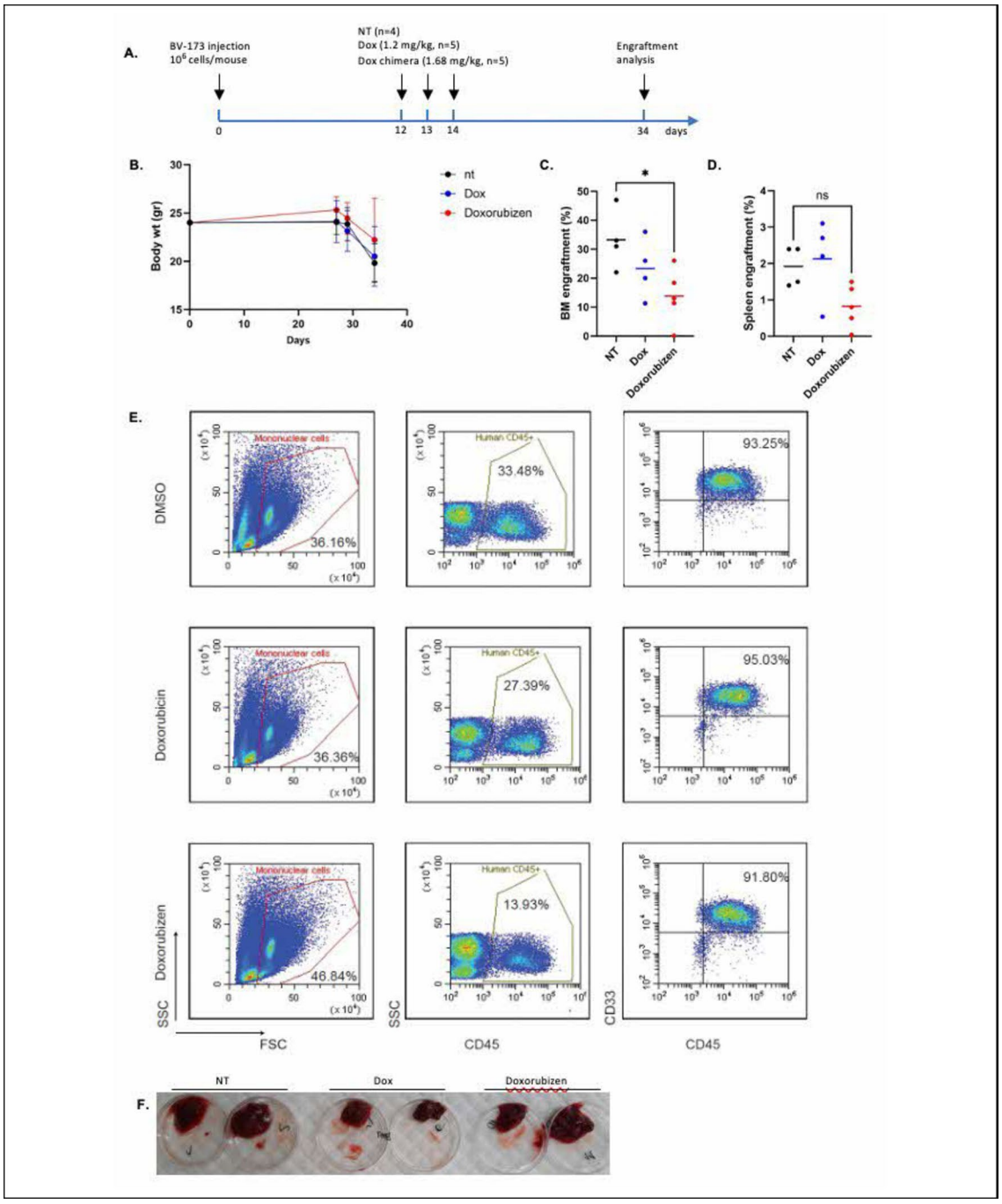

Fig. 10. **Examination of the antileukemic activity of doxorubizen** in vivo. **A**: Experimental flow chart to validate the antileukemic activity of **doxorubizen** in leukemia xenografts. **B**: Body weight of mice engrafted with BV-173 cells and exposed to chemotherapy. **C**: Leukemia burden in the bone marrow. **D**: Leukemia burden in the spleen. **E**: Flow cytometry analysis of leukemic engraftment in the bone marrow of a representative mouse from each treatment group. **F**: Representative images of whole livers dissected from solvent- and chemotherapy-exposed animals were obtained 20 days after the last drug injection. The statistical assessment was performed by one-way ANOVA ($p = 0.039$).

molecular docking analysis. Based on these binding interactions, Dox uses a sugar tether to act as both a DNA minor groove binding agent and a Topo II inhibitor. Conversely, **doxorubizen** shows a different binding mode that may also result in efficient DNA methylation. Its tetracene core interacts with DNA base pairs to help position the monomethyl triazene portion in the major groove in a way that is advantageous for methylation at the nearby nucleophilic site of the guanine base. Given that the ΔG score of do**xorubizen** is significantly greater than that of Dox, **doxorubizen** appears to be a more effective Topo II inhibitor. The role of Topo II as a target for **doxorubizen** that derived from computational modeling was confirmed by experimental validation using

a Topo II inhibition assay. Moreover, compared with Dox, **doxorubizen** was superior DNA intercalator, as it enhanced the displacement of methyl green dye from the DNA–methyl green complex. Based on the results of these studies and our previous findings (e.g., amonafidazene[10], CM358[4]), we assume that such a combined effect can be achieved only with a chimera composed of a DNA alkylating tether connected to a Topo II inhibitory DNA intercalator. According to this characteristic, methyl triazene lost its toxicity when the Dox backbone was replaced with analogs that are unable to intercalate DNA, indicating the absence of DSBs. In fact, when comparing the tested DNA non-intercalating chimeras to the parent drugs, we did not find any evidence of an increased cytotoxic effect in our investigation. Conversely, **doxorubizen** caused an increase in DSBs upon targeting with methyl triazene. As demonstrated for DNA damage by dual labeling of pH2A.X and pATM, a higher frequency of **doxorubizen**-induced DSBs and their slower repair compared to Dox-induced DSBs may be the consequence of DNA repair mechanisms interfering with one another. The methylated nucleotide repair pathways (for example, NER and BER) may obstruct the activity of the NHEJ or HR DSB repair pathways if the matching complexes assemble in close proximity to one another. Another possibility is that interactions between DNA strands are impacted by methylated thymine or guanine, which may inhibit homologous recombination (HR) repair because the process requires short complementary interactions.

In summary, our hypothesis about the mode of action of this unique chimera is supported by our computational analyses and experimental validation of the interaction between **doxorubizen** and Topo II and its potential to intercalate DNA. Biological results, including cytotoxicity assays, mitochondrial membrane potential depolarization, cell apoptosis assays, and western blot analysis of 53BP1 and p53 proteins, consistently demonstrated the clear superiority of **doxorubizen** over doxorubicin across all tested parameters. Moreover, we acknowledge the potential association of DSBs with the possibility of developing secondary cancers; therefore, the long-term consequences of **doxorubizen** administration should be investigated in future studies. Finally, in an acute leukemia xenograft model, **doxorubizen** was profoundly more effective than Dox at suppressing tumor growth, with no leukemia cells detected in a single animal, suggesting a cure.

Furthermore, we observed a reduction in liver size in all Dox-treated animals, indicating organ damage; in contrast, no appreciable alterations in liver size or form were noted in the **doxorubizen**-treated group administered the same dosage or *via* the same delivery method. We believe that the above-mentioned results justify further preclinical evaluation of **doxorubizen**.

Data availability

All data generated or analysed during this study are included in this published article and its supplementary information files.

Received: 5 September 2024; Accepted: 13 March 2025
Published online: 27 March 2025

References

1. Szumilak, M., Wiktorowska-Owczarek, A. & Stanczak, A. Hybrid drugs—A strategy for overcoming anticancer drug resistance?? *Molecules* **26**, 2601. https://doi.org/10.3390/molecules260926012 (2021).
2. de Pedrosa, O. Hybrid compounds as direct multitarget ligands: A review. *Curr. Top. Med. Chem.* **17**, 1044–1079. https://doi.org/10.2174/1568026616666160927160620 (2017).
3. Gilad, Y. et al. Discovery of potent molecular chimera (CM358) to treat human metastatic melanoma. *Eur. J. Med. Chem.* **138**, 602–615. https://doi.org/10.1016/j.ejmech.2017.06.066 (2017).
4. Walunj, D. et al. Targeted methylation facilitates DNA double strand breaks and enhances cancer suppression: A DNA intercalating/methylating dual-action chimera Amonafidazene. *Eur. J. Med. Chem.* **225**, 113811. https://doi.org/10.1016/j.ejmech.2021.113811 (2021).
5. Ohsawa, N., Yamazaki, Z., Wagatsuma, T. & Isurugi, K. Bestrabacil: a possible target-oriented anticancer agent. *Gan Kagaku Ryoho*. **11**, 2115–2124 (1984).
6. Huang, P. et al. Combination of small molecule prodrug and nanodrug delivery: amphiphilic Drug–Drug conjugate for cancer therapy. *J. Am. Chem. Soc.* **136**, 11748–11756. https://doi.org/10.1021/ja505212y (2014).
7. Haider, T., Pandey, V., Banjare, N., Gupta, P. N. & Soni, V. Drug resistance in cancer: mechanisms and tackling strategies. *Pharmacol. Rep.* **72** (5), 1125–1151. https://doi.org/10.1007/s43440-020-00138-7 (2020).
8. Mansoori, B., Mohammadi, A., Davudian, S., Shirjang, S. & Baradaran, B. The different mechanisms of cancer drug resistance: A brief review. *Adv. Pharm. Bull.* **7**, 339–334. https://doi.org/10.15171/apb.2017.041 (2017).
9. Holohan, C., Van Schaeybroeck, S. & Longley, D. B. Johnston P.G. Cancer drug resistance: an evolving paradigm. *Nat. Rev. Cancer*. **13**, 714–726. https://doi.org/10.1038/nrc3599 (2013).
10. Wang, X., Zhang, H. & Chen, X. Drug resistance and combating drug resistance in cancer. *Cancer Drug Resist.* **2**, 141–160. https://doi.org/10.20517/cdr.2019.10 (2019).
11. Berrazouane, S. et al. Beta1 integrin Blockade overcomes doxorubicin resistance in human T-cell acute lymphoblastic leukemia. *Cell. Death Dis.* **10**, 357. https://doi.org/10.1038/s41419-019-1593-2 (2019).
12. Gao, M. & Skolnick, J. A. Comprehensive survey of Small-Molecule binding pockets in proteins. *PLOS Comp. Bio*. **9** (10), e1003302. https://doi.org/10.1371/journal.pcbi.1003302 (2013).
13. Tharkar-Promod, S. et al. HDAC1,2 Inhibition and doxorubicin impair Mre11-dependent DNA repair and DISC to override BCR-ABL1-driven DSB repair in Philadelphia chromosome-positive B-cell precursor acute lymphoblastic leukemia. *Leukemia* **32**, 49–60. https://doi.org/10.1038/leu.2017.174 (2018).
14. Thankarajan, E. et al. A novel, dual action chimera comprising DNA methylating agent and near-IR xanthene-cyanine photosensitizer for combined anticancer therapy. *Photodiagn. Photodyn. Ther.* **37**, 10272. https://doi.org/10.1016/j.pdpdt.2022.102722 (2022).
15. Blyufer, A. et al. A neuroprotective drug with potential as a novel anti–cancer agent (Review). *Int. J. Oncol.* **59**, 95. https://doi.org/10.3892/ijo.2021.5275 (2021).
16. Goy, A. et al. Single-agent Lenalidomide in patients with mantle-cell lymphoma who relapsed or progressed after or were refractory to bortezomib: phase II MCL-001 (EMERGE) study. *J. Clin. Oncol.* **31**, 3688–3695. https://doi.org/10.1200/JCO.2013.49.2835 (2013).

17. Leonard, J. P. et al. AUGMENT trial investigators, AUGMENT: A phase III study of Lenalidomide plus rituximab versus placebo plus rituximab in relapsed or refractory indolent lymphoma. *J. Clin. Oncol.* **37**, 1188–1199. https://doi.org/10.1200/JCO.19.00010 (2019).
18. Schiller, G., Lee, M., Territo, M., Gajewski, J. & Nimer, S. Phase II study of Etoposide, Ifosfamide, and Mitoxantrone for the treatment of resistant adult acute lymphoblastic leukemia. *Am. J. Hematol.* **43**, 195–199. https://doi.org/10.1002/ajh.2830430307 (1993).
19. Amadori, S. et al. Mitoxantrone, Etoposide, and intermediate-dose cytarabine: an effective and tolerable regimen for the treatment of refractory acute myeloid leukemia. *JCO* **9**, 1210–1214. https://doi.org/10.1200/JCO.1991.9.7.1210 (1991).
20. Zhou, X. et al. A salvage therapy with Dara-KDT-P(A)CE in heavily pretreated, high-risk, proliferative, relapsed/refractory multiple myeloma. *Hematol. Oncol.* **40**, 202–211. https://doi.org/10.1002/hon.2949 (2022).
21. Toksvang, L. N., Lee, S. H. R., Yang, J. J. & Schmiegelow, K. Maintenance therapy for acute lymphoblastic leukemia: basic science and clinical translations. *Leukemia* **36**, 1749–1758. https://doi.org/10.1038/s41375-022-01591-4 (2022).
22. Garcia-Manero & Kantarjian, G. The hyper-CVAD regimen in adult acute lymphocytic leukemia. *Hematol. Oncol. Clin. North. Am.* **14**, 1381–1396. https://doi.org/10.1016/s0889-8588(05)70192-1 (2000). x–xi.
23. Jabbour, E. et al. Hyper-CVAD regimen in combination with ofatumumab as frontline therapy for adults with Philadelphia chromosome-negative B-cell acute lymphoblastic leukemia: a single-arm, phase 2 trial. *Lancet Hematol.* **7**, e523–e533. https://doi.org/10.1016/S2352-3026(20)30144-7 (2020).
24. Engert, A. et al. Escalated-dose BEACOPP in the treatment of patients with advanced-stage Hodgkin's lymphoma: 10 years of follow-up of the GHSG HD9 study. *J. Clin. Oncol.* **27**, 4548–4554. https://doi.org/10.1200/JCO.2008.19.8820 (2009).
25. Dunleavy, K. et al. Dose-Adjusted EPOCH-Rituximab therapy in primary mediastinal B-Cell lymphoma. *N Engl. J. Med.* **368**, 1408–1416 (2013). https://www.nejm.org/doi/10.1056/NEJMoa1214561
26. Găman, A. M., Egbuna, C. & Găman, M. A. Chap. 6 - Natural bioactive lead compounds effective against hematological malignancies, in: Egbuna, C., Kumar, S., Ifemeje, J. C., Ezzat, S. M. & Kaliyaperumal, S. (Eds.), Phytochemicals as Lead Compounds for New Drug Discovery. *Elsevier*, 95–115 (2020). https://doi.org/10.1016/B978-0-12-817890-4.00006-8
27. Emran, T. B. et al. Multidrug resistance in cancer: Understanding molecular mechanisms, Immunoprevention and therapeutic approaches. *Front. Oncol.* **12**, 916528. https://doi.org/10.3389/fonc.2022.891652 (2022).
28. Chatterjee, K., Zhang, J., Honbo, N. & Karliner, J. S. Doxorubicin cardiomyopathy. *Cardiology* **115** (2), 155–162. https://doi.org/10.1159/000265166 (2010).
29. Hughes, J., Rees, S., Kalindjian, S. & Philpott, K. Principles of early drug discovery. *Br. J. Pharmacol.* **162**, 1239–1249. https://doi.org/10.1111/j.1476-5381.2010.01127.x (2011).
30. Kuznetsov, A. V., Margreiter, R., Amberger, A., Saks, V. & Grimm, M. Changes in mitochondrial redox State, membrane potential and calcium precede mitochondrial dysfunction in doxorubicin-induced cell death. *Biochim. Biophys. Acta*. **1813**, 1144–1152. https://doi.org/10.1016/j.bbamcr.2011.03.002 (2011).
31. Eke, I. et al. 53BP1/RIF1 signaling promotes cell survival after multifractionated radiotherapy. *Nucleic Acids Res.* **48** (3), 1314–1326. https://doi.org/10.1093/nar/gkz11392024) (2020).
32. Svec, R. L. et al. Novel Imidazotetrazine evades known resistance mechanisms and is effective against Temozolomide-Resistant brain cancer in cell culture. *ACS Chem. Biol.* **17**, 299–313. https://doi.org/10.1021/acschembio.2c00022 (2022).
33. Drabløs, F. et al. Alkylation damage in DNA and RNA–repair mechanisms and medical significance. *DNA Repair. (Amst).* **3**, 1389–1140. https://doi.org/10.1016/j.dnarep.2004.05.004 (2004).
34. Scherr, M. et al. Optimized induction of mitochondrial apoptosis for chemotherapy-free treatment of BCR-ABL + acute lymphoblastic leukemia. *Leukemia* **33**, 1313–1323. https://doi.org/10.1038/s41375-018-0315-6 (2019).
35. Wunderlich, M. et al. AML cells are differentially sensitive to chemotherapy treatment in a human xenograft model. *Blood* **121**, e90–97. https://doi.org/10.1182/blood-2012-10-464677 (2013).
36. Bank, R. P. D. & Homepage, R. C. S. B. P. D. B. (n.d.). (2024). https://www.rcsb.org/(accessed January 26.
37. Wu, C. C. et al. Structural basis of type II topoisomerase Inhibition by the anticancer drug Etoposide. *Science* **333**, 459–462. https://doi.org/10.1126/science.1204117 (2011).
38. Schrödinger - Physics-based Software Platform for Molecular. Discovery & Design, (n.d.). (2024). https://newsite.schrodinger.com/(accessed January 26.
39. Mmauck Schrödinger solutions for small molecule protonation state enumeration and pKa prediction, *Schrödinger* (2023). https://newsite.schrodinger.com/materials-science/learn/white-papers/schrodinger-solutions-small-molecule-protonation-state-enumeration-and-pka/(accessed January 26, 2024).
40. Life Science. Glide, *Schrödinger* (n.d.). (2024). https://newsite.schrodinger.com/platform/products/glide/(accessed January 26.
41. Lyne, P. D., Lamb, M. L. & Saeh, J. C. Accurate prediction of the relative potencies of members of a series of kinase inhibitors using molecular Docking and MM-GBSA scoring. *J. Med. Chem.* **49**, 4805–4808. https://doi.org/10.1021/jm060522a (2006).
42. Lu, C. Improving force field accuracy on challenging regimes of chemical space. *J. Chem. Theory Comput.* **17**, 4291–4300. https://doi.org/10.1021/acs.jctc.1c00302 (2021).
43. Li, J. et al. The VSGB 2.0 model: A next generation energy model for high resolution protein structure modeling. *Proteins* **79**, 2794–2812. https://doi.org/10.1002/prot.2310644 (2011).
44. Martyna, G. J., Klein, M. L. & Tuckerman, M. Nosé–Hoover chains: the canonical ensemble via continuous dynamics. *J. Chem. Phys.* **97** (4), 2635–2643 (1992).
45. Khalifa, M. M. et al. Topo II Inhibition and DNA intercalation by new phthalazine-based derivatives as potent anticancer agents: design, synthesis, anti-proliferative, docking, and in vivo studies. *J. Enzyme Inhib. Med. Chem.* **37** (1), 299–314. https://doi.org/10.1080/14756366.2021.2007905 (2021).
46. Burres, N. S., Frigo, A., Rasmussen, R. R. & McAlpine, J. B. A colorimetric microassay for the detection of agents that interact with DNA. *J. Nat. Prod.* **55** (11), 1582–1587. https://doi.org/10.1021/np50089a004 (1992).

Acknowledgements

This research was supported by the grants ISF-1362/20 and The Varda and Boaz Dotan Research Center for Hemato-oncology Research to M.M. The authors acknowledge the Ariel HPC Center at Ariel University for providing computing resources that contributed to the research results reported in this paper. The authors are grateful to Helena Tuchinsky (Ariel University, Israel) for her kind help with the mouse experiments. The authors are grateful to Dr. Vered Marks (Ariel University) for the measurements of NMR spectra and to Dr. Itay Pitussi (Ariel University) for the measurements of HRMS spectra.

Author contributions

D.W., I.T., and A.B. were involved in the study design; synthesis and performance of the analytical experiments; data analysis; interpretation; and drafting of the manuscript. M.P. and D.T. were responsible for the modeling experiments. K.E., O. S, and O.H-R designed, performed, and analyzed all the experiments in vitro. K.E. performed and interpreted all the cell-based experiments and drafted the manuscript. S.S.N.A.M., A.Z-R., and

M.M. were involved in the design, performance, and analysis of the in vivo experiments. O.H-R., M.M., O.S, and G.G. helped to design and interpret the cell-based and animal studies. M.M., O.H-R. and G.G. designed the study, reviewed the experiments, and drafted, edited, and reviewed the manuscript. All the authors reviewed the manuscript and approved the final version.

Funding

This research was supported by the grants ISF-1362/20 (Israeli Scientific Foundation) (M.M) and The Varda and Boaz Dotan Research Center for Hemato-oncology Research, Israel (M.M).

Declarations

Competing interests

The authors declare no competing interests.

Additional information

Supplementary Information The online version contains supplementary material available at https://doi.org/10.1038/s41598-025-94373-8.

Correspondence and requests for materials should be addressed to M.M., O.H.-R. or G.G.

Reprints and permissions information is available at www.nature.com/reprints.

Publisher's note Springer Nature remains neutral with regard to jurisdictional claims in published maps and institutional affiliations.